Applied Physics A (2026) 132:471
https://doi.org/10.1007/s00339-026-09443-z

Applied Physics A
Materials Science & Processing

Quantifying selective pulsed laser cleaning and residual contamination in paper artifacts by ATR spectroscopy

Canan Yagmur Boynukara[1,2] · Valerio Graziani[3] · Mehmet Uguryol[4] · Gurcan Mavili[5] · Luca Tortora[3,6] · Andreas Ruediger[1] · Patrizio Antici[1]

Received: 16 October 2025 / Accepted: 17 February 2026
© The Author(s), under exclusive licence to Springer-Verlag GmbH Germany, part of Springer Nature 2026

Abstract
Pulsed laser cleaning of cultural heritage materials requires removing unwanted deposits from fragile substrates without inducing collateral damage. This study explores femtosecond (fs) laser cleaning of cellulose-based historical papers through a combined experimental and modeling approach. Paper samples, prepared with traditional Turkish-Ottoman sizings (alum–egg, corn starch, wheat starch) and subjected to artificial aging, were contaminated with graphite and graphite–kaolinite mixtures to replicate historical soiling. Fs laser treatments were performed within the experimentally verified safe fluence range of 0.39–0.78 J/cm^2, and the cleaning effects were monitored using Attenuated Total Reflectance Fourier Transform Infrared (ATR-FTIR) spectroscopy. The measurements demonstrated effective removal of graphite and partial reduction of kaolinite, while confirming the preservation of cellulose and sizing features. Burnished samples exhibited lower cleaning efficiency due to deeper contaminant embedding. Beyond these experiments, we introduce, for the first time in the context of paper conservation, the integration of ATR-FTIR spectroscopy with exponential saturation and decay models. This approach enables a quantitative assessment of both cleaning efficiency and residual contamination while providing predictive insight into fluence thresholds extending beyond the experimentally tested range. Overall, the combined experimental–modeling methodology establishes a robust framework for defining safe and effective fs laser cleaning parameters, offering new opportunities for the quantitative optimization of paper artifact conservation.

Keywords Femtosecond laser cleaning · Paper artifacts · ATR-FTIR spectroscopy · Exponential saturation/decay modeling

✉ Canan Yagmur Boynukara
canan.boynukara@inrs.ca

✉ Andreas Ruediger
andreas.ruediger@inrs.ca

✉ Patrizio Antici
patrizio.antici@inrs.ca

[1] INRS-EMT, 1650 Boul. Lionel-Boulet, Varennes, Québec J3X 1P7, Canada

[2] Dipartimento SBAI, Sapienza Università Di Roma, Via A. Scarpa 14, Rome 00161, Italia

[3] National Institute for Nuclear Physics (INFN) — Roma Tre Department, Via Della Vasca Navale 84, Rome 00146, Italy

[4] Department of Conservation and Restoration of Cultural Property, Faculty of Architecture, Yıldız Technical University, Besiktas, Istanbul 34349, Türkiye

[5] Department of Traditional Turkish Arts, Mimar Sinan Fine Arts University, Istanbul, Fındıklı 34427, Türkiye

[6] Department of Science, Roma Tre University, Via Della Vasca Navale 84, Rome 00146, Italy

1 Introduction

Cleaning plays an important role in the long-term preservation, legibility, and aesthetic appearance of cultural heritage objects. Artworks and artifacts face degradation due to biological (fungi, bacteria, insects), physical (temperature, humidity fluctuations), and chemical (pollutants, light, acidic inks) factors. Historical documents and paper-based artifacts are particularly vulnerable. Traditional methods for paper conservation—such as washing, alkalization, and mechanical cleaning—are widely used [1, 2]. While effective for general debris removal, these approaches require manual expertise, can be labor-intensive, and may be difficult to apply safely to fragile artifacts, such as highly degraded or embrittled papers, water-sensitive media, or documents with delicate, unstable inks. Additionally, solvent-based methods must be carefully selected to prevent

Published online: 04 May 2026

unwanted chemical interactions, and washing can risk ink loss or paper degradation.

However, conventional dry-cleaning methods struggle with contaminants that penetrate the substrate or bond chemically to the surface. While brushes, sponges, and erasers are effective for removing surface-level contaminants, they often fail when dealing with deeply embedded or chemically bonded pollutants that require selective removal. These methods can also pose risks to delicate substrates, especially when excessive mechanical force is applied. For instance, historical papers with embedded contaminants in sizing layers or intricate details are particularly challenging to clean using mechanical methods. In such cases, laser cleaning not only ensures safe and effective contaminant removal but also preserves the integrity and authenticity of these delicate substrates. Laser cleaning offers a non-contact and highly controlled alternative, minimizing physical stress on historical papers while providing selective cleaning capabilities.

Since its first use in 1971 in Venice [3], laser cleaning has become a recognized method for materials like metals, ceramics, textiles, paintings, and paper [4–9]. Its ability to partially automate the cleaning process and offer precise control has made it popular in addressing the growing demand for restoration. However, cleaning paper artifacts remains particularly challenging due to their delicate fibrous organic matrix. UV lasers, while offering precise depth control, can cause irreversible cellulose staining (yellowing) [10]. This challenge necessitates careful selection of laser parameters for successful cleaning.

Laser cleaning, a non-contact and highly controlled technique, allows adjustments in wavelength, pulse length, and polarization [11, 12]. Compared to conventional methods, it is faster, safer, and more cost-effective, making it ideal for sensitive materials [13–16]. Laser wavelengths range from infrared (IR) to ultraviolet (UV), determining penetration depth, while pulse durations, from nanoseconds to femtoseconds, affect thermal dissipation and material interaction. With nanosecond pulses, heat spreads over a larger area, while femtosecond pulses enable rapid, precise surface evaporation with minimal damage. Femtosecond infrared lasers are often preferred for cleaning paper due to their short pulse duration. Second harmonic generation, if it occurred, would provide visible light with limited consequences for photobleaching as compared to UV light [17–19].

The investigation focuses on identifying optimal fluence values for femtosecond lasers to clean model pollutants while protecting cellulose and sizing from damage. Graphite, representing soot from sources like fuel combustion or candles, absorbs infrared strongly, making it easier to remove. Kaolinite, a mineral representing dust, has weaker infrared absorption, posing challenges for selective removal.

Effective cleaning requires non-destructive methods to evaluate laser pulse effects on both contaminants and surfaces. ATR-FTIR spectroscopy and imaging offer detailed surface analysis with sufficient depth sensitivity to monitor pollutant removal and potential changes to the substrate [20, 21]. This analytical capability is particularly crucial for understanding the interaction of laser parameters with historical materials.

In this study, ATR-FTIR spectroscopy (4000–400 cm^{-1}) is used to track the laser cleaning of artificially soiled paper samples and assess cellulose quality. Infrared spectroscopy identifies vibrational signatures unique to contaminants, sizing, and cellulose, enabling precise analysis of cleaning progress and residual contamination.

Focusing on samples modeling Turkish-Ottoman manuscripts, the research highlights the use of "ahar," a sizing that improves paper uniformity, smoothness, and glare while preventing ink spreading and excessive absorption. It also enhances ink flow, enabling corrections and creating better writing conditions. Effective laser cleaning of Ottoman paper artifacts requires optimizing parameters to accommodate both the paper and sizing properties.

This study builds upon previous research by integrating ATR-FTIR spectroscopy with a saturation model to quantify cleaning efficiency and substrate preservation. Unlike existing studies, which often focus on visual or morphological assessments, this approach provides detailed chemical insights into the cleaning process, enabling precise evaluation of contaminant removal and substrate integrity. By establishing laser fluence thresholds specific to cellulose-based historical papers, this work offers a novel framework for safe and effective laser cleaning, contributing to the preservation of delicate cultural heritage materials.

The present work aims to define optimized laser cleaning parameters for cellulose-based mock-up papers representative of Turkish-Ottoman artifacts, by establishing minimum and maximum intensity thresholds for selective contaminant removal and identifying conditions for multiple laser pulse applications. The comparative models are designed to evaluate the response of cellulose-based paper samples, treated with various traditional sizing types, to femtosecond laser cleaning. By integrating ATR-FTIR spectroscopy with mathematical fitting techniques, including exponential saturation and decay models, these models quantify cleaning efficiency and residual contamination. Comparing different laser cleaning conditions across sample treatments allows for the identification of key factors influencing contaminant removal and substrate preservation, providing a framework for safe and effective restoration practices.

To achieve this goal, comparative models are developed to analyze how contaminated and aged paper samples respond to laser cleaning, laying the foundation for effective

and controlled cleaning techniques. All the artificially produced samples for this research are prepared considering the most common sizing types in the Turkish-Ottoman archives, i.e., alum-egg, corn starch, and wheat starch.

2 Methods

2.1 Paper samples

As previously stated, laser cleaning relies on the absorption of laser pulse energy, translating into heat on the surface. This process depends heavily on the absorption properties of molecular species present in significant quantities. Thus, understanding the surface properties enhances the precision of the cleaning process. Information about previous chemical or mechanical treatments can be gathered through historical documentation (e.g., conservation reports), scientific analysis (e.g., spectroscopy), or material testing and should be evaluated before cleaning.

Variables considered in this study include paper sizing, burnishing, and contamination type. Alum-egg, corn starch, and wheat starch sizing—common in Turkish-Ottoman manuscripts—were selected for sample preparation. Samples without sizing were also included. All sizing types were applied wet to paper using a brush and burnished after drying, following traditional methods. Burnishing, a historical treatment, involves rubbing the surface of the paper with a smooth, rounded tool, often made of glass or a glassy rock known as mühre. This process applies consistent pressure while the paper rests on a rigid plane, enhancing surface smoothness and uniformity. In this study, burnishing was conducted using a glass burnisher to replicate historical practices. Unburnished samples were also prepared to evaluate the potential differences attributed to this treatment.

Two types of contamination were selected: graphite and a graphite-kaolinite mixture (1:1 mass ratio). Graphite powder (AF spezial, Kropfmühl, D90≤25 microns) was used as a surrogate for the carbon-dominated fraction of soot and char associated with fossil fuel combustion, candles, and oil lamps that are relevant to historical periods or fires. This model contamination does not include the organic components present in real soot, but it offers a reproducible and well-controlled approximation of the highly absorbing particulate fraction. Kaolinite, a clay mineral, represents dust from natural rock weathering and silica-containing man-made materials like concrete or cement. These particles could stem from building materials or storage environments such as gardens or unpaved roads. Although kaolinite is occasionally used as a filler in paper manufacturing [22, 23], preliminary ATR-FTIR analysis confirmed that the acid-free calligraphy papers used in this study do not exhibit any of the characteristic kaolinite bands (see Supplementary Document). Contaminants were manually applied by brush to simulate environmental contamination in a controlled setup for studying laser cleaning efficiency. Contaminated samples were burnished to enhance adhesion, and one sample without sizing was burnished post-contamination to promote deeper penetration.

Figure 1 illustrates the sample preparation combinations. Detailed procedures are provided in [24]. Finally, all samples were aged under conditions specified in standards ASTM D 4714 T and TAPPI 544 cm-08 at 90 °C and 50% relative humidity for 16 days, corresponding to a humid-heat accelerated aging protocol rather than a typical library storage climate. Aging conditions improved sizing distribution and promoted contaminant penetration into surface voids. The aging conditions applied to the samples were selected to accelerate the natural degradation and pollutant adhesion processes that occur in historical paper artifacts over time. Elevated temperature and controlled moisture content promote the migration of sizing components and contaminants into the paper fibers, creating a more realistic and challenging scenario for laser cleaning. This increased adhesion of pollutants to the substrate allows for a more accurate evaluation of laser cleaning efficiency, particularly in distinguishing between the removal of surface contaminants and those embedded within the paper structure. By replicating such conditions, this study ensures that the findings are relevant to real-world applications involving aged and contaminated paper artifacts.

2.2 Femtosecond (fs) laser cleaning setup

A Yb: Glass chirped-pulse amplification system at 1030 nm center wavelength (Amplitude Systems, s-Pulse) was used to clean, producing pulses with a 550 fs pulse duration and 1 kHz repetition rate. The maximum pulse energy is approximately 250 µJ. The sample was mounted on an XYZ stage, and the laser was focused onto the surface by a 25 mm focal length cylindrical lens (Fig. 2). During cleaning, the samples were translated under the focused beam at a scanning speed of 1 mm/s with a pitch of 0.5 mm. All parameters were kept constant during all fs laser cleaning. The number of pulses delivered per spot was determined by the chosen scanning speed and pitch. Incubation effects and cumulative pulse interactions were not varied in this study. Six fluence values ranging from 0.39 to 0.78 J/cm^2 were chosen by changing the beam's energy over a fixed surface of the paper samples. The selection of fluence values for the fs laser setup was based on preliminary experimental trials rather than direct literature sources. Average laser power was varied between 100 and 200 mW in 20 mW increments, and the corresponding fluence

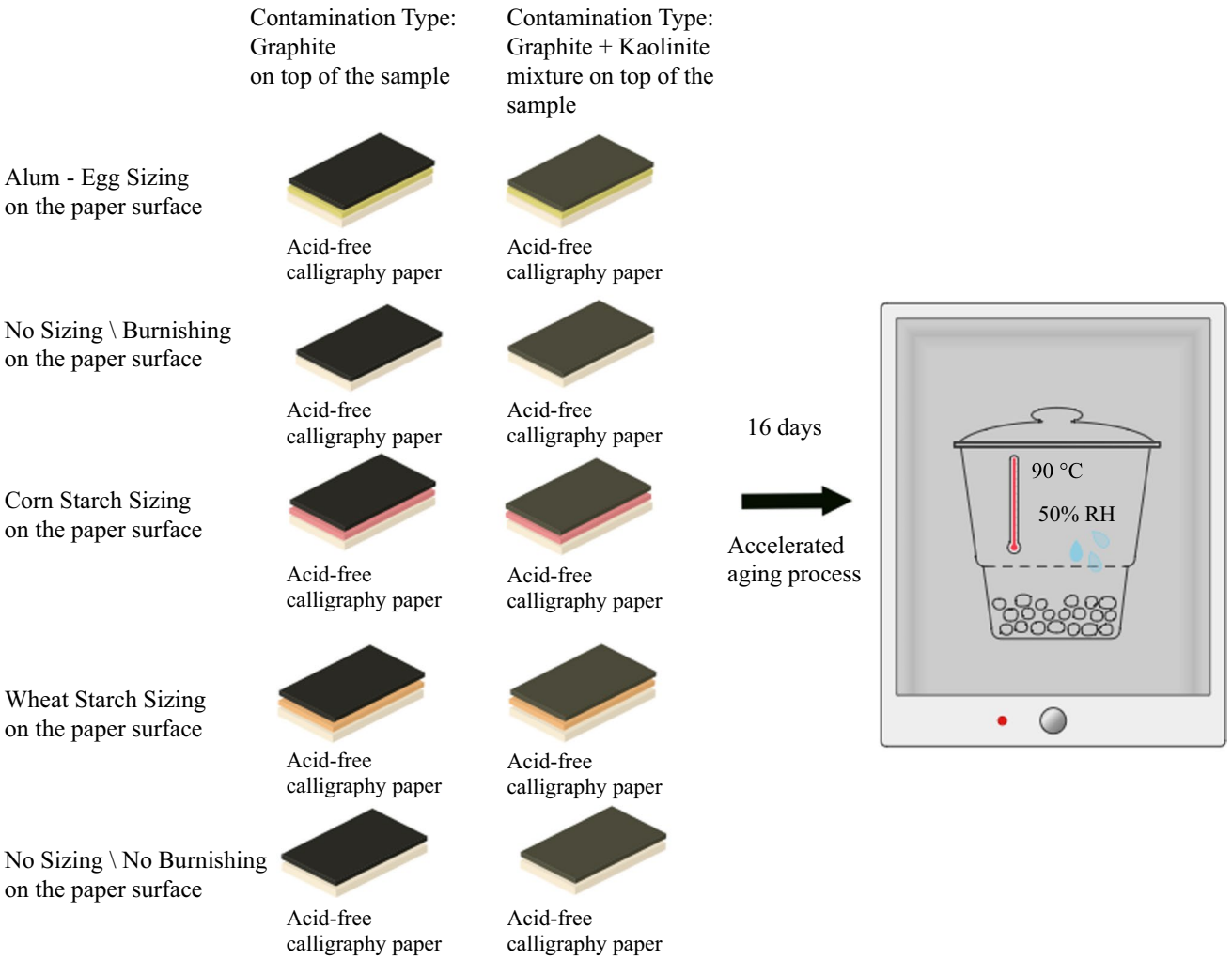


Fig. 1 Overview of sample preparation and artificial aging protocol

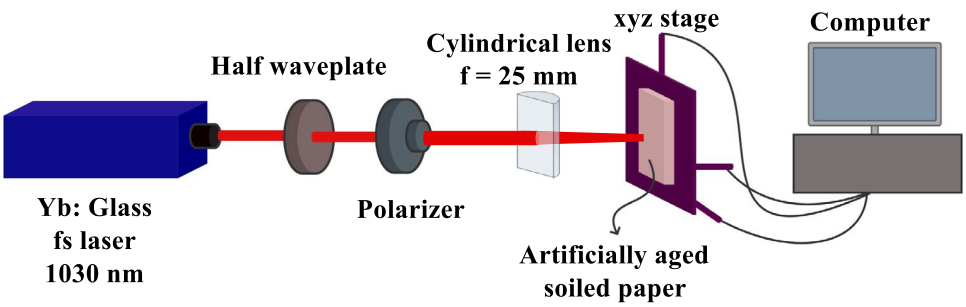


Fig. 2 Schematic of the femtosecond laser cleaning setup

values (0.39 to 0.78 J/cm^2) were calculated based on the beam area. The beam area was determined from direct observation of the line-focused beam footprint (beam height × waist) at the sample plane. The waist is defined as the diameter at which, within the peak, the fluence drops by 1/e^2. As the resulting profile is non-Gaussian, the fluence values reported are specific to this configuration and are not intended for direct inter-laboratory comparison. This range was determined empirically to achieve effective contaminant removal while avoiding visible surface alterations, thus aligning with the study's objective of identifying safe and efficient cleaning parameters for cellulose-based paper samples. The upper limit of 0.78 J/cm^2 was set near the threshold where minor substrate degradation could occur, allowing for an evaluation of cleaning efficiency at higher intensities. Conversely, the lower limit of 0.39 J/cm^2 represents the minimum fluence required to observe noticeable cleaning effects.

A set of six square-shaped cleaned areas, each measuring 15×15 mm^2, were realized on the paper surface. This was achieved using a cylindrical lens, which focuses the beam along the x-axis, allowing for sharp, well-defined edges during square-pattern scanning.

2.3 Scanning electron microscopy

A Tescan Vega3 LMH Scanning Electron Microscope was used to analyze the surface morphology of the samples. For these measurements, an accelerating voltage of 10 kV was applied for samples covered by graphite and kaolinite, with a working distance of approximately 17 mm.

2.4 Stylus profilometry

A KLA Tencor P-7 Stylus Profilometer was used to measure the surface roughness of the samples. For these measurements, the scan length was set as 1000 µm, the scan speed as 50 µm\sec, and the sampling rate as 200 Hz. The applied force was chosen as 1.5 mN, at the lower end of stylus tracking forces, to limit damage to the sample surface.

2.5 Attenuated total reflectance (ATR) spectroscopy

ATR spectroscopy measurements were performed using a Thermo Fisher Nicolet™ iS50 FTIR Spectrometer equipped with an Attenuated Total Reflectance (ATR) mode analysis compartment. The system consists of a diamond crystal and a 45° IR incident beam, with only one internal reflection and a controlled contact force to provide reproducible contact between the diamond crystal and the surface. The active surface is a few mm^2. Absorbance spectra were collected in the range 4000–400 cm^{-1}, corresponding to the mid-infrared region and including the "fingerprint" region. The spectral resolution was 4 cm^{-1}. Each spectrum resulted from the accumulation of 64 scans. The background spectrum was obtained through an acquisition in air and used for subsequent numerical corrections.

2.6 Data collection and processing

Profilometer measurements were conducted in triplicate for each contamination type to assess adhered contamination and its impact on surface properties. The averaged data provided a representative evaluation for each sample.

Scanning electron microscopy (SEM) was performed at a 45° angle with a magnification of ~5000x. To prevent charging, clean, aged, and contaminated samples (graphite and kaolinite) were coated with a 4 nm Pt/Pd alloy layer using a sputter coater before imaging.

ATR measurements were taken at three equidistant points (upper, middle, and lower parts, width: 5 mm) in the cleaned zone (see red dots in Fig. 6). Repeated measurements allowed data averaging and error calculation. Error bars in figures reflect uncertainties from these points. ATR corrections, using a refractive index of 1.50, and baseline corrections were applied to all spectra.

The analysis focused on spectral regions with significant modifications from cleaning, identifying peaks corresponding to contaminants (e.g., kaolinite) or substrates (e.g., cellulose, corn starch, wheat starch in graphite-only cases). Contaminant band intensities were expected to decrease, while substrate intensities increased with cleaning. Contamination intensity refers to the spectral signal of materials like kaolinite or graphite, while substrate intensity reflects underlying materials such as cellulose or starches. Overlapping features in cellulose, polysaccharide-based sizings, and kaolinite spectra were carefully accounted for in peak selection. Since alum-egg sizing peaks were indistinguishable from cellulose, cellulose peaks were tracked for this sizing. Table 1 presents the intervals (peaks) for each paper treatment case. ATR-FTIR analysis encompassed key spectral regions for cellulose (~850–1200 cm^{-1}), contaminants (e.g., kaolinite, graphite), and sizing agents (e.g., starches, alum-egg). Across all components, no significant spectral shifts were observed post-cleaning, confirming the chemical integrity of the substrate. The quantitative evaluation focused on changes in peak intensities to assess cleaning efficiency and substrate preservation rather than shifts in peak positions.

The baseline-corrected integrated absorbance area over each selected interval in Table 1 is denoted as A(x), where x is the laser fluence, and A(x) is reported in arbitrary units. The absolute magnitude of A(x) depends on the selected band and preprocessing, and therefore should not be interpreted as an absolute reflectance or absorbance value directly comparable across different materials. For example, in alum–egg sizing sample contaminated with graphite, A(x) is extracted from a cellulose-dominated interval

Table 1 Chosen intervals for each paper treatment

Sizing	Contamination type	Chosen intervals	
alum – egg	graphite	~850–1200 cm^{-1}	(cellulose)
alum – egg	graphite + kaolinite	~500–550 cm^{-1}	(kaolinite)
no sizing	graphite	~800–1200 cm^{-1}	(cellulose)
no sizing	graphite + kaolinite	~500–550 cm^{-1}	(kaolinite)
corn starch	graphite	~500–550 cm^{-1}	(corn starch)
corn starch	graphite + kaolinite	~3600–3650 cm^{-1}	(kaolinite)
wheat starch	graphite	~500–550 cm^{-1}	(wheat starch)
wheat starch	graphite + kaolinite	~3600–3650 cm^{-1}	(kaolinite)

around 850–1200 cm^{-1}, whereas for alum–egg sizing sample contaminated with graphite + kaolinite, A(x) is extracted from a kaolinite-dominated interval around 500–550 cm^{-1}. Because these intervals correspond to different vibrational bands with different intrinsic intensities, A(x) values can differ substantially in magnitude even when the fluence-dependent cleaning progression is comparable. Repeated measurements were used to calculate the standard deviation and the standard error of the mean, which are shown as error bars in the graphs (Fig. 7 and 8).

Figures 3 and 4 illustrate examples of this process, showing the numerically integrated peaks for cellulose and kaolinite, respectively. The shaded areas represent the spectral regions over which integration was performed. In both figures, the shaded region corresponds to the integrated peak area A(x) that is used as the input quantity in the exponential saturation (Eq. (1)) and decay (Eq. (2)) models.

To evaluate laser cleaning effectiveness, ATR peak areas were analyzed as a function of laser fluence. Once cleaning has started, each additional increase in fluence acts on a progressively smaller amount of removable material: a fraction of the contamination has already been removed, and a fraction of the substrate has already been exposed. As a result, the incremental effect of further fluence becomes smaller, and the signal approaches an asymptotic value. This first-order type of behavior is well captured by an exponential approach to saturation or decay, which motivates the use of the following phenomenological models.

For quantifying cleaning efficiency, we used an exponential saturation model described by Eq. (1):

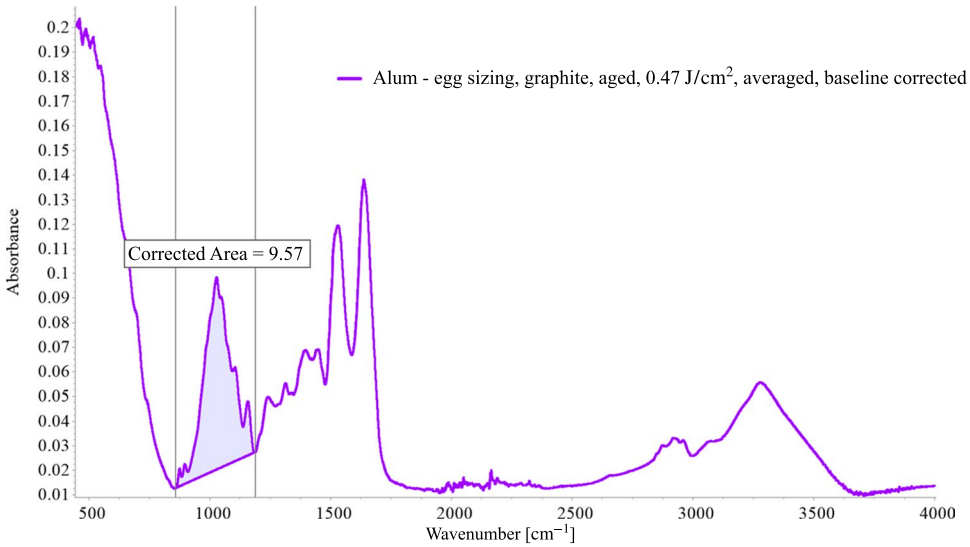


Fig. 3 ATR-FTIR spectrum averaged from three measurements and baseline-corrected, showing the integrated absorbance peak of cellulose (shaded area) used for quantitative analysis. The 'Corrected Area' label indicates the numerically integrated region A(x). The sample is alum–egg sized paper contaminated with graphite, aged, and cleaned at 0.47 J/cm^2

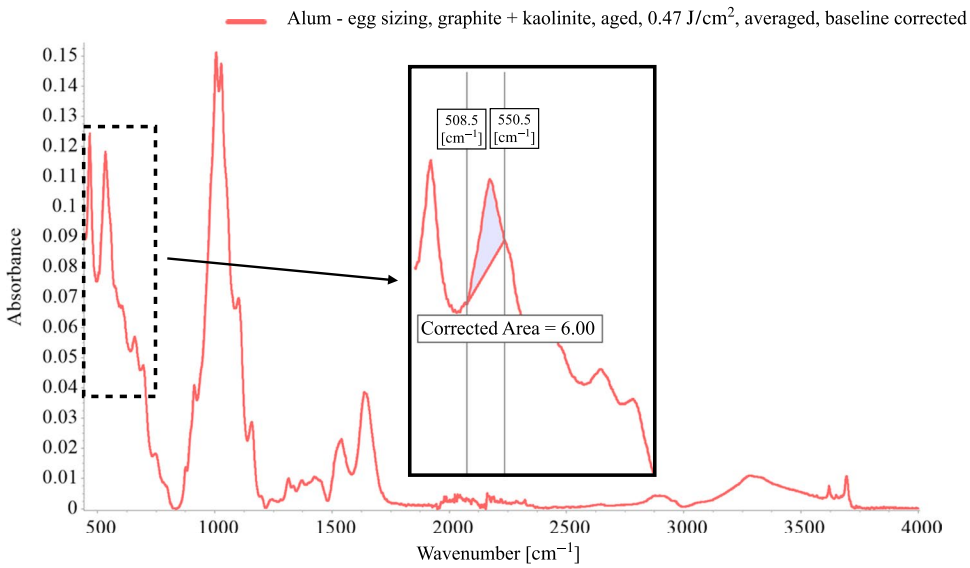


Fig. 4 ATR-FTIR spectrum averaged from three measurements and baseline-corrected, showing the integrated absorbance peak of kaolinite (shaded area) used for quantitative analysis. The 'Corrected Area' label indicates the numerically integrated region A(x). The sample is alum–egg sized paper contaminated with graphite + kaolinite mixture, aged, and cleaned at 0.47 J/cm^2

$$A(x) = a \cdot \left(1 - e^{-\frac{(x-b)}{c}}\right) + d \quad (1)$$

where A(x) is the area at laser fluence x, *a* is the maximum possible area, *b* is the fluence offset, which is strictly positive as cleaning for negative laser fluences would yield unphysical interpretations, *c* is the saturation constant, and *d* is the baseline offset.

The model assumes an asymptotic maximum area (a) beyond which additional fluence does not significantly increase cleaning efficiency and a fluence offset (b) indicating the minimum threshold fluence required to initiate cleaning. The saturation constant (c) reflects how quickly the process reaches saturation, and the baseline offset (d) accounts for any initial signal before cleaning. Using MATLAB, we performed non-linear least squares fitting with initial parameter guesses based on preliminary observations. The fitting process involved iteratively adjusting the parameters to minimize the difference between observed data and model predictions, and the fit quality was evaluated using metrics such as the coefficient of determination (R^2), root mean square error (RMSE), and mean absolute error (MAE). The fitted parameters provided insights into the cleaning efficiency, highlighting the optimal fluence range for effective cleaning.

In this work, the saturation fluence F_{sat} is defined as the fluence at which the fitted saturation model reaches 99% of its asymptotic change. For Eq. (1), the asymptotic value is $A_\infty = a + d$, and the 99% criterion corresponds to $A(F_{\text{sat}}) = d + 0.99\,a$. Solving Eq. (1) gives: $F_{\text{sat}} = b - c\ln(0.01)$. This 99% criterion is used as a practical definition of the plateau regime, meaning that only 1% of the remaining change toward the asymptote is left, and further increases in fluence lead to negligible additional variation in A(x).

For quantifying residual contamination, we applied the exponential decay model, described by Eq. (2):

$$A(x) = a \cdot \left(e^{-\frac{(x-b)}{c}}\right) + d \quad (2)$$

where A(x) is again the area at laser fluence x, *a* is the initial area representing the contamination level, *b* is the fluence offset, which is again strictly positive, *c* is the decay constant, and *d* is the baseline offset.

This model assumes that the area under the peak representing contaminant concentration decreases with increasing fluence but almost never reaches zero, as some residual contamination is expected to remain in the voids of the surface. Using MATLAB, we performed non-linear least squares fitting with initial parameter guesses based on preliminary observations. The fitting process involved iteratively adjusting the parameters to minimize the difference between observed data and model predictions, and the fit quality was evaluated using the same metrics as for the saturation model. The fitted parameters allowed us to estimate the residual contamination and assess the effectiveness of different laser cleaning conditions. Both models provided valuable insights into the cleaning and contamination processes, enabling us to quantify and compare the efficacy of varying laser cleaning conditions.

The saturation fluence F_{sat} is defined as the fluence at which the fitted decay model reaches 99% of its asymptotic minimum. For Eq. (2), the asymptotic minimum is $A_\infty = d$. Completing 99% of the decay is equivalent to the remaining exponential contribution being 1% of its initial amplitude, i.e., $A(F_{\text{sat}}) = d + 0.01\,a$. Substituting this condition into Eq. (2) gives: $F_{\text{sat}} = b - c\ln(0.01)$. This definition marks the plateau regime, meaning that only 1% of the modeled change remains, and further increases in fluence produce negligible additional variation in A(x) relative to the experimental variability.

3 Results

3.1 Surface morphology by scanning microscope

Corn and wheat starch sizing are fine, white powders commonly dispersed in water to form non-Newtonian suspensions or pastes, which are then applied to paper surfaces. Once dried, these sizings create thin, translucent films that enhance the paper's strength, smoothness, and resistance to ink penetration. In contrast, alum-egg sizing, a unique blend of alum (aluminum potassium sulfate) and egg white (albumen), offers a slightly viscous or gel-like consistency.

Scanning electron microscopy (SEM) images in Fig. 5 reveal that unsized samples a) exhibit more irregularities and gaps between paper fibers compared to those treated with alum-egg b) and corn starch sizing c). Wheat starch-sized samples contaminated with graphite d) and graphite+kaolinite e) display additional surface features linked to contaminants. Although the SEM image for wheat starch sizing is not shown in Fig. 5, it is available in Supplementary Materials, where it demonstrates behavior similar to corn starch sizing. Alum-egg sizing, due to its gel-like consistency, penetrates and adheres to paper fibers more effectively than other sizings, resulting in a smoother surface texture and reduced irregularities.

SEM images of wheat starch samples contaminated with graphite d) and graphite+kaolinite e) show that the mixture forms a more uniform and continuous layer compared to graphite alone, filling gaps between fibers more effectively. Additional SEM images are available in the Supplementary Materials to confirm consistency across measurements.

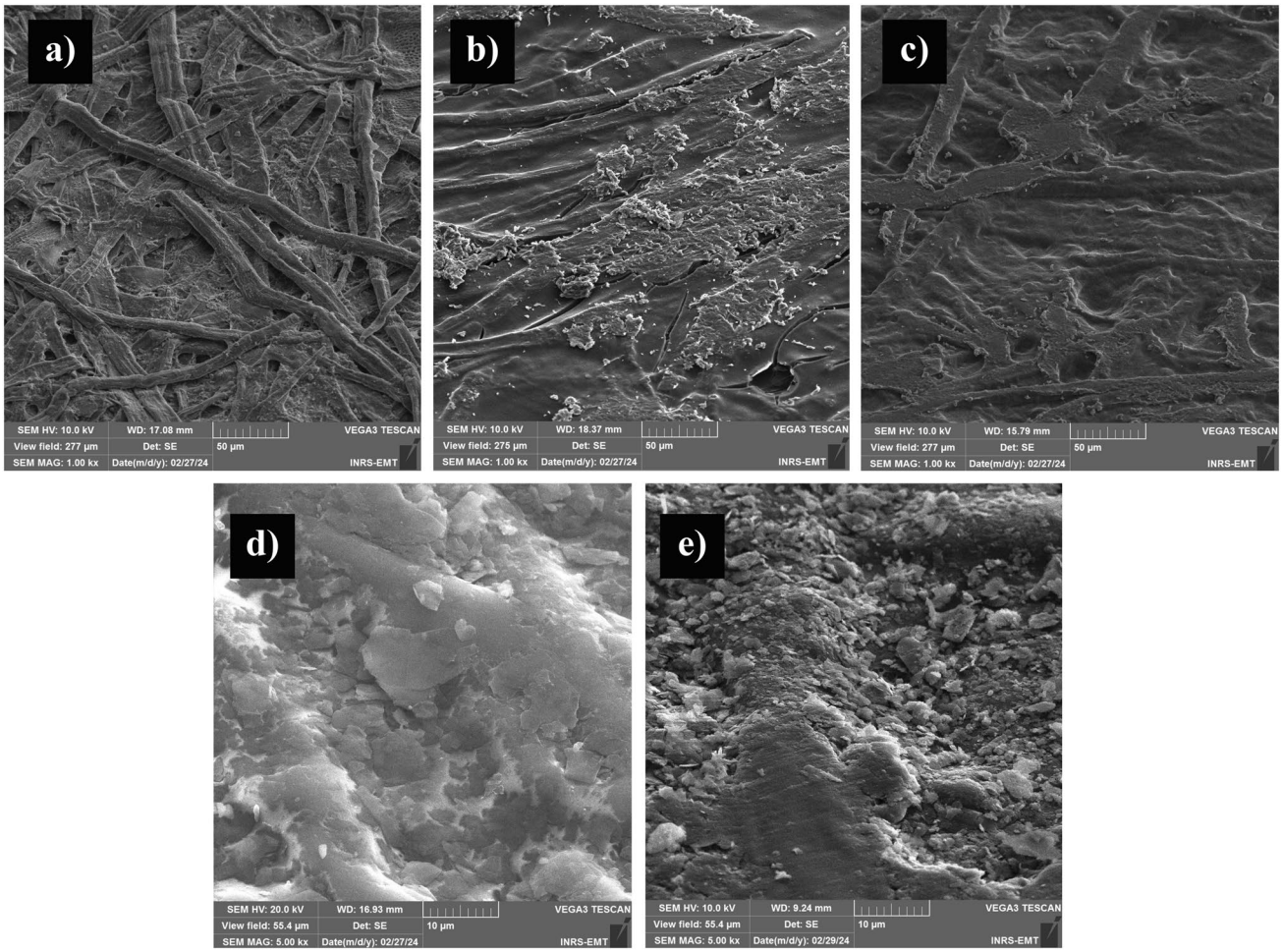


Fig. 5 Scanning electron microscopy (SEM) images of paper samples taken after aging but before contamination and cleaning: **a**) no sizing, **b**) alum-egg sizing, **c**) corn starch sizing. SEM images also show wheat starch-sized samples contaminated with **d**) graphite and **e**) graphite + kaolinite

3.2 Surface roughness

Profilometer data in Table 2 indicate increased surface roughness in graphite-contaminated samples compared to those with graphite + kaolinite, with one exception in the alum-egg-sized sample, where graphite + kaolinite contamination resulted in higher surface roughness. The surface roughness measurements presented in Table 2 focus on initial conditions prior to cleaning, aiming to evaluate the influence of sizing and contamination on surface morphology. While variability in measurements exists, these values provide a critical context for understanding contaminant adhesion and substrate preparation.

Table 2 Average roughness values of the different paper treatments

	Contamination type	
Samples	Graphite	Graphite + kaolinite
no sizing/no burnishing	1.9 ± 0.6 µm	1.7 ± 0.3 µm
no sizing/burnishing	1.9 ± 0.9 µm	1.1 ± 0.5 µm
alum – egg sizing	0.6 ± 0.2 µm	1.2 ± 0.6 µm
wheat starch sizing	1.6 ± 0.8 µm	1.5 ± 0.6 µm
corn starch sizing	1.9 ± 1.0 µm	1.6 ± 0.3 µm

On the other hand, graphite + kaolinite-contaminated samples exhibit lower roughness, indicating smoother surfaces and better contaminant infiltration into paper pores. Kaolinite appears to enhance contaminant penetration into the substrate, complicating cleaning processes like laser cleaning. Deeper contamination reduces laser interaction with embedded particles, making removal more challenging. SEM images in Fig. 5(d and e) corroborate these findings, visually highlighting smoother surfaces and reduced irregularities in graphite + kaolinite contaminated samples compared to graphite alone.

Samples without sizing and burnishing show the highest roughness, while burnished samples without sizing exhibit reduced roughness regardless of contamination type. The absence of sizing, which fills surface pores, and burnishing, which compacts the surface, explains these variations. Table 2 shows that corn starch sizing consistently produces the highest roughness across contamination types, followed by

wheat starch and alum-egg sizing. The consistently higher surface roughness observed in corn starch sizing can be attributed to its unique molecular composition. Corn starch is primarily composed of amylose and amylopectin, the latter being highly branched, leading to less uniform film formation upon application. This irregular distribution creates microscale variations on the paper surface, contributing to increased roughness. Additionally, the gelatinization and retrogradation behaviors of starch, influenced by its amylose-to-amylopectin ratio, play a role in surface morphology. Such behaviors have been reported to affect the texture and film uniformity of starch-based coatings [25, 26]. Furthermore, corn starch tends to form a more superficial layer compared to other sizings, such as alum-egg, which penetrates the paper fibers more effectively. This combination of structural and application-specific factors explains the higher roughness values observed in corn starch sizing across all contamination types. While roughness measurements clarify the effects of burnishing and sizing types, the combined impact of contamination and sizing on roughness remains ambiguous. These observations underline the complex interactions between sizing, contaminant behavior, and surface roughness, emphasizing their influence on the effectiveness of laser cleaning for paper substrates.

The preservation of surface morphology of these samples after femtosecond laser cleaning has been demonstrated in a previous study [24], where microscopy images confirmed that no damage occurred under the laser parameters used (1030 nm, 300 fs, 1 kHz, 100–200 mW). As the same samples were used in this study, the findings regarding surface preservation remain valid.

3.3 Quantifying cleaning with saturation modeling

Figure 6 shows the areas cleaned with the femtosecond laser at different fluences. The image provides a visible indication of progressive laser cleaning, and while an investigation into the recovery of the paper color might be possible, determining the overall condition is difficult without knowing the initial color of the paper. For that matter, we decided to pursue a spectroscopic approach that traces the relative intensities of infrared absorption lines for both contaminants and sizings.

The following section will discuss the experimental findings based on a saturation model, leading to a specific relation between laser fluence and recovered substrate signal or contamination. While there is a multitude of different mathematical relations that may qualify for fitting, we justify the use of our model through the nature of the interaction between the laser and surface absorbers. The more material that has been removed, the lower any further interaction between laser and absorber will be, and since the total absorption coefficient is linear in the concentration of the remaining absorbers on the surface, we anticipate the exponential relationships that are the basis of our numerical treatment in the following section.

Figure 7 illustrates the fitting curve for the exponential saturation model applied to alum-egg sizing with graphite contamination during fs laser cleaning. The results indicate that the area under the peak increases with increasing fluence, eventually reaching a saturation point beyond which further increases in fluence do not significantly affect the area.

The graph demonstrates how the signal attributed to alum-egg sizing, representing the substrate's relative concentration in the ATR spectra, increases with fluence until it reaches a saturation value of 14.69 a.u. at a saturation fluence of 1.12 J/cm^2. The fit quality metrics (R^2=0.9552, RMSE=0.5005, MAE=0.3055) indicate a strong correlation between the model and the experimental data. A higher R^2 value close to 1 suggests a well-fitting model, while lower RMSE (Root Mean Square Error) and MAE (Mean Absolute Error) indicate minimal deviations between the predicted and observed values. In modeling, we also explored the fluence value below, in which no visible cleaning effect occurs by extrapolation towards lower fluences. This value was calculated by finding the fluence at which the fitted curve's area under the curve approaches zero. During this fitting process, constraints were applied to ensure that the fluence (x) was not a complex number, negative, or greater than 0.39 J/cm^2. For this specific example, the value was determined to be 0.31 J/cm^2. Below this fluence, no cleaning for the given configuration should be expected, even for multiple consecutive pulses.

The fitted parameters for the other samples, based on the exponential saturation model, and their proximity to saturation are listed in Table 3.

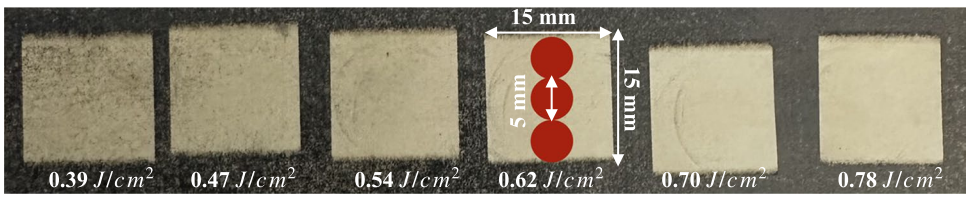


Fig. 6 Cleaned regions of artificially soiled and aged paper (alum-egg sizing, graphite+kaolinite contamination). Square areas were cleaned with the fs laser at 1030 nm. Red spots represent the data collecting points for ATR measurements. Progressive cleaning success with increasing laser fluence is visible; however, it is hardly quantifiable

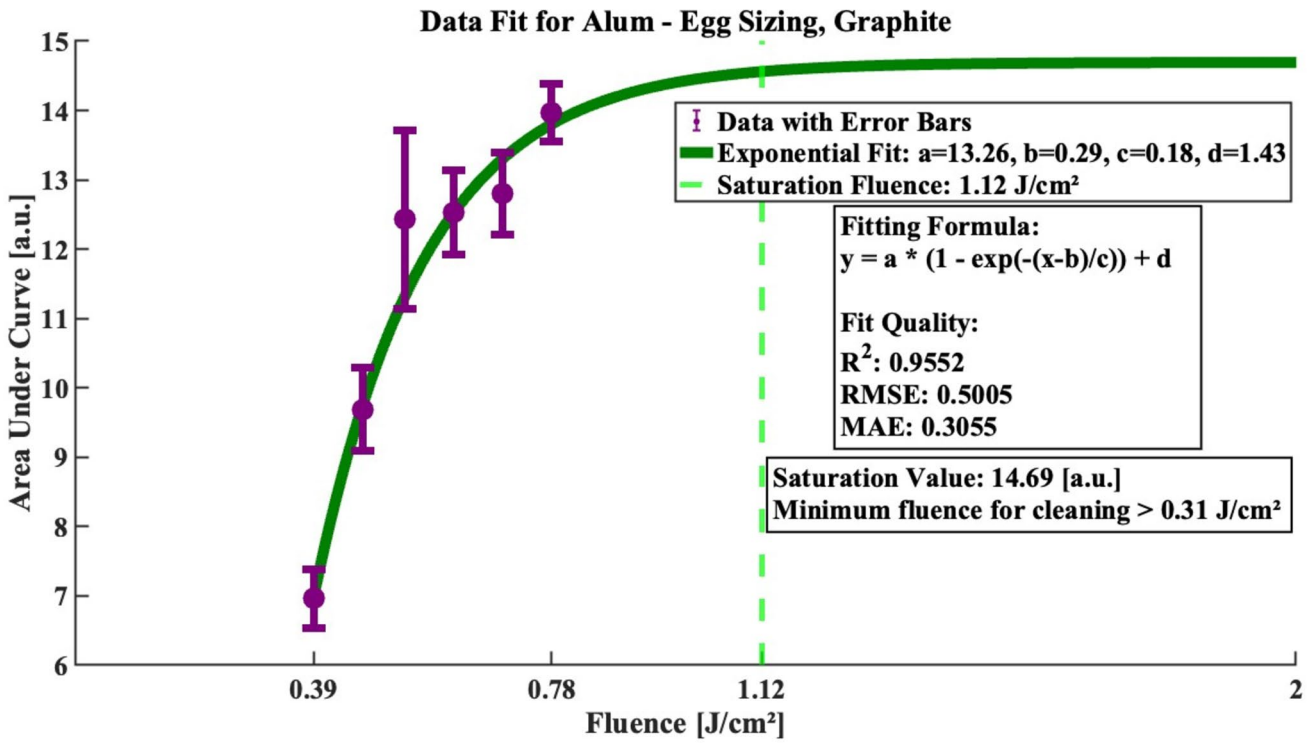


Fig. 7 Exponential saturation model fit for alum-egg sizing with graphite contamination for fs laser cleaning. The green solid curve represents the fitted cleaning trajectory, and the vertical green dashed line marks the saturation fluence threshold (1.12 J/cm^2) determined from the model. Beyond this fluence value, the model extrapolates the cleaning response. However, prediction uncertainty increases as the curve extends beyond the range of measured data

Table 3 Fitted parameters for exponential saturation model and saturation proximity

Sample	Saturation fluence [J/cm^2]	Minimum fluence for cleaning [J/cm^2]	R^2	RMSE	MAE
wheat starch sizing	2.70	>0.38	0.9630	0.0135	0.0126
alum – egg sizing	1.12	>0.31	0.9552	0.5005	0.3055
corn starch sizing	0.96	>0.37	0.9548	0.4642	0.0178
no sizing/burnishing	1.79	>0.29	0.9177	1.2317	0.9312
no sizing/no burnishing	1.24	>0.27	0.9711	0.7496	0.4320

3.4 Estimating residuals via decay modeling

The exponential decay model results demonstrate that the area under the peak representing contaminant concentration decreased with increasing fluence but did not reach zero, indicating residual contamination. Figure 8 shows the fitting curve for the exponential decay model for corn starch sizing with graphite contamination for fs laser cleaning.

Figure 8 illustrates how the area under the curve decreases with fluence until it approaches a saturation value of 3.12×10^{-12} a.u. at a saturation fluence of 1.26 J/cm^2. The fit quality metrics (R^2=0.9724, RMSE=0.8830, MAE=0.0020) demonstrate a good fit between the model and the experimental data, accurately capturing the decay process. Complete contamination removal is unlikely except for excessively high laser fluences beyond the destruction threshold of the cellulose (around 1 J/cm^2) or multiple pulsing.

The fitted parameters for the other samples, based on the exponential decay model, and their proximity to saturation are listed in Table 4.

The parameters in Tables 3 and 4 quantify the laser cleaning efficiency. In Table 3, saturation fluence refers to the fluence at which the cleaning response reaches its plateau, providing a practical benchmark for comparing how quickly different surfaces approach maximum cleaning. SEM analysis in Supplementary Material Fig. 3 supports the interpretation of these trends, showing that fiber compaction by burnishing reduces porosity, embeds contaminants more deeply, and lowers per-pulse removal efficiency.

Threshold fluences also varied. Among sized samples, alum–egg required the lowest threshold (~0.31 J/cm^2),

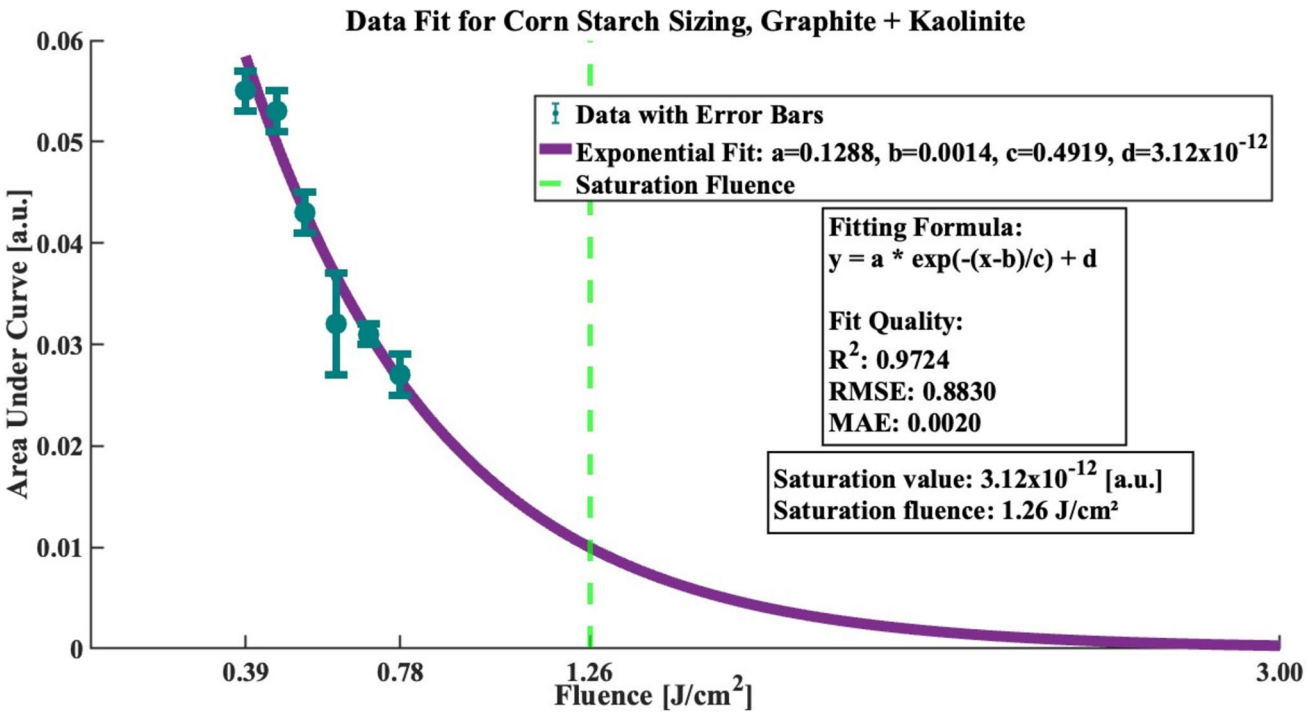


Fig. 8 Exponential decay model fit for corn starch sizing with graphite + kaolinite contamination for fs laser cleaning

Table 4 Fitted parameters for exponential decay model and saturation proximity

Sample	Saturation fluence [J/cm^2]	R^2	RMSE	MAE
corn starch sizing	1.26	0.9724	0.8830	0.0020
wheat starch sizing	0.96	0.9152	1.3524	0.0066
alum – egg sizing	2.93	0.9868	0.9652	0.0596
no sizing/burnishing	2.08	0.9427	1.8776	0.0303
no sizing/no burnishing	2.28	0.9885	1.5753	0.0700

followed by corn starch (~0.37 J/cm^2) and wheat starch (>0.38 J/cm^2). For no sizing samples, burnishing again raised the threshold: 0.27 J/cm^2 without burnishing versus > 0.29 J/cm^2 with burnishing.

The decay-model results in Table 4 provide an additional view of cleaning performance by quantifying the removal and residual contamination after cleaning. The fitted saturation fluence values highlight additional contrasts: wheat starch required the least fluence (0.96 J/cm^2), corn starch was intermediate (1.26 J/cm^2), while alum–egg demanded the most (2.93 J/cm^2). No sizing samples showed still higher fluence needs (2.08–2.28 J/cm^2), reflecting deeper contaminant penetration in the absence of sizing.

Overall, both models underline that cleaning efficiency depends on chemical composition (sizing type) and physical surface state (burnishing). Quantitative parameters such as saturation fluence, threshold fluence, and residual contamination provide practical benchmarks for optimizing laser cleaning while safeguarding the substrate.

4 Discussion

When evaluating the models regarding contamination, we observe systematic differences between the exponential saturation and exponential decay descriptions. The exponential saturation model reflects the response of the substrate beneath the graphite contamination, indicating that graphite is efficiently removed from the surface due to its strong, broad-band absorption. In contrast, the exponential decay model directly tracks the graphite and kaolinite mixture, which exhibits greater resistance to fs laser cleaning than graphite alone. This observation aligns with the optical absorption spectra of the materials: graphite strongly absorbs across the visible and NIR spectral range [27], whereas kaolinite, though transparent in the visible region, has low absorption at 1030 nm [28]. Scanning electron microscopy (SEM) images and profilometer measurements confirm that the graphite and kaolinite mixture forms a more uniform and continuous layer in the paper fibers, making it more challenging to clean compared to graphite alone.

The parameters in Tables 3 and 4, such as “saturation fluence”, are crucial for evaluating laser cleaning efficiency.

Saturation fluence indicates the fluence level at which the cleaning response approaches a plateau, meaning that further increases do not lead to a substantial additional cleaning effect. Together with threshold behavior and the decay-model outcomes, these parameters provide practical benchmarks for comparing cleaning performance across surface conditions and sizing types, while maintaining the balance between effective contaminant removal and substrate preservation.

Burnishing significantly impacts laser cleaning. Compared to the no sizing and no burnishing condition, burnishing compacts the fibrous network and promotes deeper embedding of contamination, which reduces effective laser interaction per pulse and makes the removal process less efficient. In practical terms, burnishing tends to "rub in" the contamination and increases the difficulty of cleaning, consistent with the morphological evidence observed by SEM and profilometry.

Quantitative analysis offers valuable insights from experimental data. It enables the estimation of key parameters such as the maximum substrate signal recoverable (asymptotic saturation), residual contamination concentration, and the minimum laser fluence required for effective cleaning. Furthermore, knowing the saturation value helps determine how much of the ideal cleaning has been achieved and whether the conditions for complete cleaning are feasible without exceeding the destruction threshold of the substrate. Together, these analyses provide practitioners with a framework to establish meaningful experimental parameters.

This study demonstrates the potential of femtosecond laser cleaning as an effective and selective restoration technique for cellulose-based historical papers. By integrating ATR-FTIR spectroscopy with exponential saturation and decay models, we quantified cleaning efficiency and substrate preservation. The results identified a safe fluence range (0.39–0.78 J/cm^2) for the specific paper substrates and contaminant systems investigated. This range was supported by experimental observations and further validated by modeling, which predicted saturation fluence values no lower than approximately 0.96 J/cm^2. Controlled laser treatment effectively addressed even challenging contaminants like kaolinite, achieving near-contaminant-free surfaces with minimal residuals. It should be noted that the conclusions drawn regarding cleaning thresholds and safe fluence ranges are specific to the pulse overlap conditions, as well as the contamination and sizing types considered in this study. Incubation-related threshold variations were not the focus of this work, having been deliberately excluded to maintain controlled and consistent exposure parameters.

For practical applications, preliminary cleaning tests should prioritize non-invasive methods to assess substrate response. These tests could involve gradually increasing fluence and pulse counts within the identified safe range, coupled with real-time monitoring techniques like ATR-FTIR or microscopic imaging, to optimize cleaning while preserving the substrate. Such protocols would ensure safe and effective restoration tailored to the specific characteristics of historical artifacts.

While this study provides valuable insights into femtosecond laser cleaning parameters for cellulose-based historical papers, several limitations should be acknowledged. The models used simplify the complex interactions between the laser and heterogeneous substrates, which may influence the accuracy of predictions. Additionally, variations in sample preparation, such as sizing distribution and pollutant application, could affect the reproducibility of results. The use of artificially soiled samples, while controlled, may not fully replicate the complexities of naturally aged artifacts. Future research should focus on addressing these limitations by incorporating naturally aged samples, exploring advanced modeling techniques, and standardizing sample preparation protocols to improve reproducibility and real-world applicability.

Overall, this study establishes a system-specific framework for developing safe and efficient laser cleaning methods that balance cleaning effectiveness with substrate preservation.

Supplementary Information The online version contains supplementary material available at https://doi.org/10.1007/s00339-026-09443-z.

Acknowledgements The authors thank Dr. Catalin Harnagea (INRS-EMT, Research Associate) for performing the SEM measurements and Dr. Marco Ruggieri (Roma Tre University) for conducting the stylus profilometry measurements.

Funding This work was supported by the Natural Sciences and Engineering Research Council of Canada (NSERC) (Grant — RG-PIN-2023-05459, ALLRP 556340 – 20) and the Digital Research Alliance of Canada (Job: pve-323-ac). A.R. gratefully acknowledges an NSERC discovery grant RGPIN-2024-06730, and A.R. and P.A. are grateful for generous funding through an NSERC Alliance /Prima Québec (R27-46-012-PME) project.

Data availability The datasets generated and/or analyzed during the current study are not publicly available but are available from the corresponding author upon reasonable request.

Declarations

Competing interests All the authors declare no competing financial or non-financial interests.

References

1. S. Zervos, I. Alexopoulou, Paper conservation methods: a literature review. Cellulose **22**, 2859–2897 (2015)
2. F. Di Turo, The chemistry behind paper restoration: diagnostic techniques and cutting-edge innovation. ChemTexts **11**, 7 (2025)
3. J.F. Asmus, C.G. Murphy, W.H. Munk, Studies on the interaction of laser radiation with art artefacts. Proc. SPIE **41**, 19–27 (1973)
4. P. Boonrat, M. Dickinson, M. Cooper, Initial investigation into the effect of varying parameters in using an Er:YAG laser for the removal of brass-based overpaint from an oil-gilded frame. J. Inst. Conserv. **43**, 1–13 (2020)
5. J.M. Larson, M. Cooper, S. Sportun, Developments in the application of laser technology for conservation. Stud. Conserv. **45**(sup1), 107–110 (2000)
6. T. Ersoy, T. Tunay, M. Uguryol, G. Mavili, S. Akturk, Femtosecond laser cleaning of historical paper with sizing. J. Cult. Herit. **15**, 259–265 (2013)
7. M. Bertasa, C. Korenberg, Successes and challenges in laser cleaning metal artefacts: a review. J. Cult. Herit. **53**, 100–117 (2022)
8. C. Chillè, G. Rossignoli, T. Nagasawa, I. Osticioli, J. Agresti, S. Siano, D. Ciofini, Laser cleaning of artificially soiled cotton fabric: assessment of surface chemical effects. J. Cult. Herit. **62**, 15–24 (2023)
9. A. Zanini, L. Bartoli, The laser as a tool for the cleaning of cultural heritage. IOP Conf. Ser. Mater. Sci. Eng. **364**, 012078 (2018)
10. P. Rudolph, F. Ligterink, J. Pedersoli et al., Laser-induced alteration of contaminated papers. Appl. Phys. A **79**, 941–944 (2004)
11. E. Zekou, I. Tsilikas, E. Chatzitheodoridis, A.A. Serafetinides, Laser paper cleaning: the method of cleaning historical books. Proc. SPIE **10226**, 1022605 (2017)
12. J. Brand, A. Wain, A.V. Rode, S. Madden, L. Rapp, Towards safe and effective femtosecond laser cleaning for the preservation of historic monuments. Appl. Phys. A **129**, 246 (2023)
13. P. Pouli, in *Laser Cleaning on Stonework: Principles, Case Studies, and Future Prospects*, eds. By F. Gherardi, P.N. Maravelaki Conserving Stone Heritage. Cultural Heritage Science (Springer, Cham, 2022).
14. P. Pouli, M. Oujja, M. Castillejo, Practical issues in laser cleaning of stone and painted artefacts: optimisation procedures and side effects. Appl. Phys. A **106**, 447–464 (2012). https://doi.org/10.1007/s00339-011-6696-2
15. S. Siano, J. Agresti, I. Cacciari et al., Laser cleaning in conservation of stone, metal, and painted artifacts: state of the art and new insights on the use of the Nd:YAG lasers. Appl. Phys. A **106**, 419–446 (2012)
16. P. Pouli, K. Melessanaki, V. Tornari, E. Bernikola, G. Filippidis, D. Anglos, C. Fotakis, An integrated approach to the study and preservation of paintings using laser light technology: diagnosis, analysis and cleaning, in *Science and Art: The Painted Surface*. (Royal Society of Chemistry, Cambridge, 2014), pp.287–313
17. S. Pentzien, A. Conradi, R. Koter, J. Krüger, Cleaning of artificially soiled paper using nanosecond, picosecond, and femtosecond laser pulses. Appl. Phys. A **101**, 441–446 (2010)
18. J. Kolar, M. Strlič, S. Pentzien, W. Kautek, Near-UV, visible and IR pulsed laser light interaction with cellulose. Appl. Phys. A **71**, 87–90 (2000)
19. P. Rudolph, F.J. Ligterink, J.L. Pedersoli Jr., M. van Bommel, J. Bos, H.A. Aziz, J.B.G.A. Havermans, H. Scholten, D. Schipper, W. Kautek, Characterization of laser-treated paper. Appl. Phys. A **79**, 181–186 (2004)
20. D. Thickett, B. Pretzel, FTIR surface analysis for conservation. Heritage Sci. **8**, 5 (2020)
21. G.-L. Liu, S.G. Kazarian, Recent advances and applications to cultural heritage using ATR-FTIR spectroscopy and ATR-FTIR spectroscopic imaging. Analyst **147**, 1777 (2022)
22. W.M. Bundy, J.N. Ishley, Kaolin in paper filling and coating. Appl. Clay Sci. **5**, 397–420 (1991)
23. M.A. Hubbe, J.J. Pawlak, A.A. Koukoulas, Paper's appearance: a review. BioResources **3**(2), 627–665 (2008)
24. C.Y. Boynukara, M. Uguryol, G. Mavili, S. Akturk, An investigation of the cleaning performances of femtosecond and nanosecond laser pulses for artificially soiled papers with sizing. Appl. Phys. A **127**, 275 (2021)
25. R.F. Tester, W.R. Morrison, Swelling and gelatinization of cereal starches. Cereal Chem. **67**, 558–563 (1990)
26. J. Jane, Structural features of starch granules part II. J. Appl. Glycosci. **56**, 105–112 (2009)
27. T. Smausz, B. Kondász, T. Gera, T. Ajtai, N. Utry, M. Pintér, G. Kiss-Albert, J. Budai, Z. Bozóki, G. Szabó, B. Hopp, Determination of UV–visible–NIR absorption coefficient of graphite bulk using direct and indirect methods. Appl. Phys. A **123**, 633 (2017)
28. J.D. Lindberg, M.S. Smith, Visible and near infrared absorption coefficients of Kaolinite and related clays. Am. Mineral. **59**, 274–279 (1974)

Publisher's Note Springer Nature remains neutral with regard to jurisdictional claims in published maps and institutional affiliations.

Springer Nature or its licensor (e.g. a society or other partner) holds exclusive rights to this article under a publishing agreement with the author(s) or other rightsholder(s); author self-archiving of the accepted manuscript version of this article is solely governed by the terms of such publishing agreement and applicable law.